COUPLED FINITE ELEMENT MODEL FOR AN AFM CANTILEVER BEAM INCLUDING A PIEZOCERAMIC BASE ACTUATOR

Kleber dos Santos Rodrigues [1], **Marcelo Areias Trindade** [1]

[1] São Carlos School of Engineering, Av. Trabalhador São Carlense, 400, 13566-590, São Carlos, SP, Brazil, kleber_sr@hotmail.com, trindade@sc.usp.br

Abstract: The modeling and analysis of the Atomic Force Microscope (AFM) cantilever beam is essential to understand and to improve its operation. With approximately $140\mu m$, the cantilever beam has a probe tip at its free end, and, at the clamped end, a PZT actuator is responsible to excite (depending on the operation mode) and move it in xyz directions. While the probe tip scans the sample surface, a laser beam detects its deflections sending a signal to a photo detector. Several operation modes may be used, depending on the sample characteristics and desired analysis. The tapping mode is a common operation mode, in which the cantilever beam vibrates in a frequency close to its resonance and softly touches the sample surface, while a feedback control system through the piezoceramic actuator is designed to keep the probe tip-sample distance constant. The error between desired and achieved probe tip-sample distances is evaluated and minimized. Thus, the necessary quasi-static base motion is obtained and used to determine the topology of the sample surface. However, due to tip-sample nonlinear interaction forces, the feedback control system may become unable to find the required base motion and, hence, from the point-of-view of the end user, the topology of the sample surface, observed as a coloured pixel in a sample image, is poorly detected. Normally, this occurrence is identified by an abnormal image constructed by the xy plane pixels obtained from the AFM. In this work, the piezoceramic base actuator and the cantilever beam are modeled using the finite element method leading to a coupled system. Material and geometric properties of the cantilever beam and probe tip are obtained from a real AFM device, which enables the model validation. The tip-sample interactions are modeled using Lennard Jones potentials and numerical simulations are performed to understand the effects of changing the tip-sample distance, as well as the effects of changing the number of vibration modes of the cantilever beam.

Keywords: Piezoeletric coupling, Finite Element Model, Atomic Force Microscope, Nonlinearities, Cantilever beam

INTRODUCTION

One of the main features of the Atomic Force Microscope (AFM) is the ability to measure a wide range of properties of surfaces with nanometer order sizes. Using the pair cantilever-probe, it is possible to obtain 3D images of nanoscale sample topology. From this point of view, the AFM working process has become a topic widely studied in recent years. According to Jalili and Laxminarayana (2004), modeling and analysis of the AFM system is essential to improve its operation.

In the specific literature, several mathematical models are developed to represent the system composed of cantilever beam, probe tip and base excitation. In most part of them, the system is modeled using 1 or 2-dof spring-mass-damper system (Dankowicz, 2006; Misra et al., 2008; Nozaki et al., 2010; Rodrigues et al., 2011; Tusset et al., 2013). Another approach is to use beam theories to represent the AFM cantilever beam, such as Bernoulli-Euler (Rodrigues et al., 2014; Rutzel et al., 2003; Stark et al., 2004), and Timoshenko (Claeyssen, 2010; Hsu et al., 2007). Some of the disadvantages of these previous approaches are that more complex beam geometries and boundary conditions are not accounted for and it is more difficult to perform parametric analysis and design.

In this paper, the aim is to model an AFM system using the finite element method to represent the system composed of cantilever beam, clamped-PZT-base and free end (tip mass and interaction forces). Numerical simulations are used, first, to validate the model, through comparison with experimental results, and, then, to help understand the system behavior under variation of the number of vibration modes, considered in the reduced model, and tip-sample distance.

MATHEMATICAL MODELING

This section aims to develop a mathematical model to represent the AFM system composed by the cantilever beam and its free and clamped ends. As seemed in the figure 1, at the clamped end ($x = 0$), a PZT (Lead Zirconate Titanate) piezoelectric ceramic actuator, responsible for the cantilever beam motion in z-direction will be considered. At the free end ($x = L$), a tip mass, representing the probe tip, and points transversal force, representing the interaction between probe and sample surface, are considered.

The AFM cantilever beam is modeled as a standard Bernoulli-Euler beam finite element model. It is also considered a

probe tip with mass m_t and inertia moment I_t at its free end. At the clamped end, it is considered that the cantilever beam is perfectly coupled with a PZT actuator. The cantilever beam is also considered to be homogeneous and uniform with length L_s, width b_s, thickness h_s, cross-section second moment of area I_s and made of a material with Young's modulus E_s, Poisson's ratio ν_s and mass density ρ_s. At the free end, an interaction force f_t, represented by Lennard Jones Potentials is also considered. The probe tip is initially set at a distance d from the sample surface.
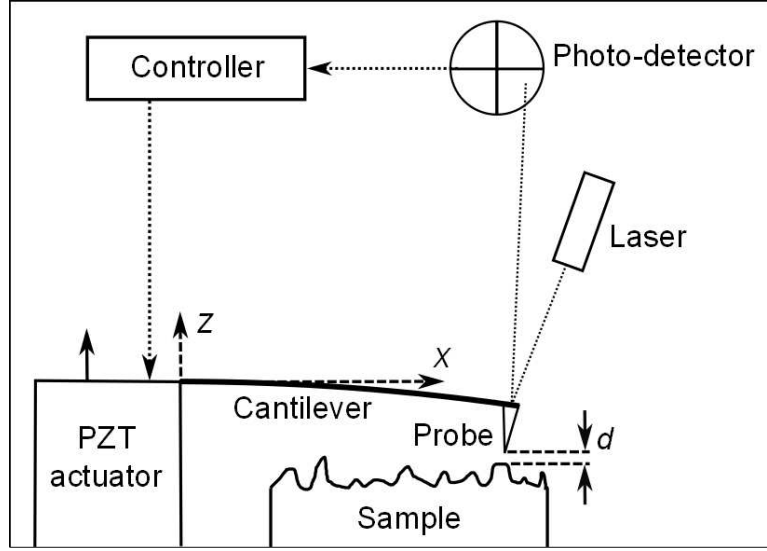

Figure 1 – AFM scheme

The tip deflections are detected by a laser beam that sends a signal to a photo detector. The acquired signal is then compared to a constant value by a feedback control system, that point-to-point corrects this z value generating the local pixel. Considering the standard Bernoulli-Euler hypothesis for a slender beam in xz plane deflection, the displacements field may be written as

$$\bar{u}(x,y,z,t) = -zw'(x,t), \ \bar{v}(x,y,z,t) = 0, \ \bar{w}(x,y,z,t) = w(x,t), \tag{1}$$

where w is the transverse displacement (in z-direction) and $w' = \partial w / \partial x$ is the cross-section rotation angle.

Based on these kinematic hypotheses, the only non-null mechanical strain, that is the normal longitudinal strain ε_{s_x}, can be written from the usual strain-displacement relation as

$$\varepsilon_{s_x} = -zw''. \tag{2}$$

Hermite cubic shape functions are assumed for the discretization of the transverse deflection $w(x,t)$, along the element length L_{s_e}, such that a two node finite element with two degrees of freedom per node, namely deflection w_i and cross-section rotation angle w'_i ($i = 1, 2$), is obtained as shown in Fig. 2.
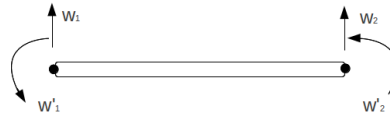

Figure 2 – Bernoulli-Euler beam finite element.

The elementary degrees of freedom (dof) column vector $\mathbf{u}_e$ is defined as

$$\mathbf{u}_e = \begin{bmatrix} w_1 & w'_1 & w_2 & w'_2 \end{bmatrix}^t, \tag{3}$$

and the transverse relative displacement of the cantilever can be written in terms of the elementary dof's as

$$w(x,t) = \mathbf{N}_s(x)\mathbf{u}_e(t). \tag{4}$$

Using Eq. 2, the normal strains can be discretized and written in terms of the elementary dof as

$$\varepsilon_{s_x} = -z\mathbf{B}_s\mathbf{u}_e, \ \text{with} \ \mathbf{B}_s = \mathbf{N}_s''. \tag{5}$$

At $x = L_s$, the cantilever beam is considered free, with actuation of interaction forces that will be properly modeled in the next section. At $x = 0$, a sliding free boundary condition with $w'(0,t) = 0$ is considered. Later on, the left-end transversal displacement $w(0,t)$ will be defined as coincident to the PZT actuator longitudinal displacements $u_p(t)$. Figure 3 represents a simple scheme of the cantilever beam taking into account a PZT actuator in the clamped end, where u_p is the cantilever beam base displacement due to the deformation suffered by the PZT actuator.
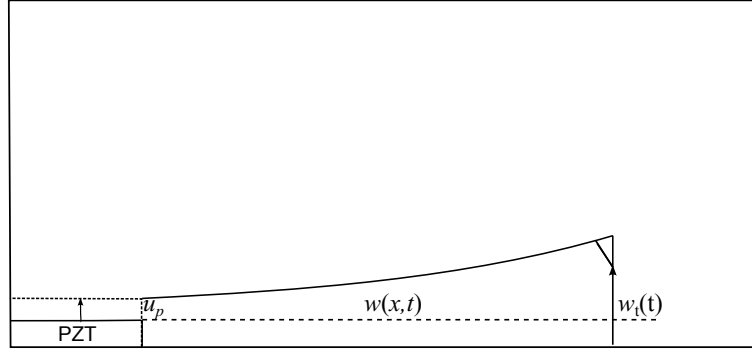
Figure 3 – Schematic representation of the cantilever beam coupled to a PZT actuator.

The virtual variation of kinetic and potential energies may be written in terms of the elementary nodal dof vector as

$$\int \delta T_{s_e}\,\mathrm{d}t = - \int \delta \mathbf{u}_e^{\mathrm{t}}\mathbf{M}_{s_e}\ddot{\mathbf{u}}_e\,\mathrm{d}t, \quad \delta U_{s_e} = \delta \mathbf{u}_e^{\mathrm{t}}\mathbf{K}_{s_e}\mathbf{u}_e, \tag{6}$$

where $\mathbf{M}_{s_e}$ and $\mathbf{K}_{s_e}$ are the elementary mass and stiffness matrices defined by

$$\mathbf{M}_{s_e} = \int_0^{L_{se}} \rho_s A_s \mathbf{N}_s^{\mathrm{t}}\mathbf{N}_s\,\mathrm{d}x \quad \text{and} \quad \mathbf{K}_{s_e} = \int_0^{L_{se}} E_s I_s \mathbf{B}_s^{\mathrm{t}}\mathbf{B}_s\,\mathrm{d}x \tag{7}$$

Accounting to the probe-tip at the free end of the cantilever beam and writing the deflection $w(L,t)$ and cross-section rotation angle $w'(L_s,t)$ of the probe tip as function of the global nodal dof vector, follows that

$$w(L,t) = \mathbf{L}_w\mathbf{u} \quad \text{and} \quad w'(L,t) = \mathbf{L}_{wx}\mathbf{u}, \quad \text{with} \quad \mathbf{L}_w = \begin{bmatrix} 0 & \cdots & 0 & 1 & 0 \end{bmatrix} \quad \text{and} \quad \mathbf{L}_{wx} = \begin{bmatrix} 0 & \cdots & 0 & 1 \end{bmatrix}. \tag{8}$$

Hence, the equivalent mass matrix corresponding to the probe tip, $\mathbf{M}_t$, is written as

$$\mathbf{M}_t = \mathbf{L}_w^{\mathrm{t}}m_t\mathbf{L}_w + \mathbf{L}_{wx}^{\mathrm{t}}I_t\mathbf{L}_{wx}. \tag{9}$$

Using Eq. 9, the total mass matrix of the cantilever beam will be represented as $\mathbf{M}_{T_s} = \mathbf{M}_s + \mathbf{M}_t$.

For the PZT piezoelectric ceramic actuator, it is considered a unidimensional longitudinal (in z-direction) deformation and for which the internal (potential) energy can be represented by electric enthalpy, written in terms of the normal longitudinal (in z-direction) elastic strain ε_{p_3} and electric field E_{p_3}, such that

$$\delta H(\varepsilon_{p_3}, D_{p_3}) = \delta\varepsilon_{p_3}\sigma_{p_3} - \delta E_{p_3}D_{p_3} \longrightarrow \begin{cases} \sigma_{p_3} = c_{p_{33}}^E \varepsilon_{p_3} - e_{p_{33}}E_{p_3} \\ D_{p_3} = e_{p_{33}}\varepsilon_{p_3} + \epsilon_{p_{33}}^{\varepsilon}E_{p_3} \end{cases} \tag{10}$$

where σ_{p_3} is the mechanical stress, D_{p_3} is the longitudinal electric displacement, $c_{p_{33}}^E$ is the effective elastic stiffness coefficient (at constant electric field), $e_{p_{33}}$ is the effective piezoelectric coefficient and $\epsilon_{p_{33}}^{\varepsilon}$ is the dielectric permittivity (at constant strain). The virtual variation of potential energy for the PZT actuator may be written as

$$\delta U_p = \int \left(\delta\varepsilon_{p3}c_{p_{33}}^E \varepsilon_{p3} - \delta\varepsilon_{p3}e_{p_{33}}E_{p3} - \delta E_{p3}e_{p_{33}}\varepsilon_{p3} - \delta E_{p3}\epsilon_{p_{33}}^{\varepsilon}E_{p3} \right)\,\mathrm{d}\Omega. \tag{11}$$

Assuming uniform mechanical strain and electric fields along the longitudinal direction, also defining h_p as the PZT height and u_p as the longitudinal displacement of the actuator at the end fixed to the cantilever beam, such that $\varepsilon_p = \dfrac{u_p}{h_p}$ and $E_3 = \dfrac{V}{h_p}$, the integration of Eq. 11 over the PZT volume leads to

$$\delta U_p = \delta u_p k_{pm}u_p - \delta u_p k_{pp}V_p - \delta V_p k_{pp}u_p - \delta V_p k_{pe}V_p, \tag{12}$$

where $k_{pm} = \dfrac{c^E_{p_{33}} A_p}{h_p}$, $k_{pp} = \dfrac{e_{p_{33}} A_p}{h_p}$ and $k_{pe} = \dfrac{\epsilon^\varepsilon_{p_{33}} A_p}{h_p}$ are the elastic, piezoelectric and dielectric stiffnesses.

The virtual variation of the kinetic energy of the PZT actuator is written assuming that its total longitudinal displacement in z direction is $\bar{u}_p(z) = z\dfrac{u_p}{h_p}$, such that

$$\int \delta T_p \, dt = -\int \int \delta \bar{u}_p \rho_p \ddot{\bar{u}}_p \, d\Omega \, dt. \tag{13}$$

After integration over the PZT actuator volume, Eq. 13 may be written as

$$\int \delta T_p \, dt = -\int \delta u_p \frac{m_p}{3} \ddot{u}_p \, dt, \tag{14}$$

where $m_p = \rho_p A_p h_p$ is the PZT actuator mass. Since PZT will serve only as an actuator, it follows that the electric voltage V_p is prescribed, so that $\delta V_p = 0$, and, thus,

$$\delta U_p = \delta u_p k_{pm} u_p - \delta u_p k_{pp} V_p. \tag{15}$$

EQUATIONS OF MOTION FOR THE COUPLED SYSTEM

Based on previous virtual variations of kinetic and potential energies and work done by external forces, for the cantilever beam and PZT actuator, the extended Hamilton's principle for the coupled system may be written as

$$\int \left(\delta T_s + \delta T_p - \delta U_s - \delta U_p + \delta W \right) dt = 0 \tag{16}$$

where $\int \delta T_s = \int \delta \mathbf{u}^t \mathbf{M}_{T_s} \ddot{\mathbf{u}} \, dt$, $\delta U_s = \delta \mathbf{u}^t \mathbf{K}_s \mathbf{u}$, $\delta W = \delta \mathbf{u}^t \mathbf{F}_t$ and δT_p and δU_p are defined in Eqs. 14 and 15 respectively.

Considering that $w(0,t) = u_p(t) = \mathbf{L}_p \mathbf{u}$ and $w'(0,t) = 0$, where $\mathbf{L}_p = [1\ 0 \cdots 0]$, the equations of motion for the coupled system can be written as

$$\left(\mathbf{M}_{T_s} + \mathbf{M}_p \right) \ddot{\mathbf{u}} + \left(\mathbf{K}_s + \mathbf{K}_p \right) \mathbf{u} = \mathbf{F}_p + \mathbf{F}_t \tag{17}$$

where

$$\mathbf{M}_p = \mathbf{L}_p^t \frac{m_p}{3} \mathbf{L}_p, \quad \mathbf{K}_p = \mathbf{L}_p^t k_{pm} \mathbf{L}_p, \quad \mathbf{F}_p = \mathbf{L}_p^t k_{pp} V_p \quad \text{and} \quad \mathbf{F}_t = \mathbf{L}_w^t f_t. \tag{18}$$

As stated above, f_t represent the tip-sample interaction forces, that in this case, will be represented using the Lennard Jones potentials. According to (Israelachvli, 1991) may be written as

$$f_t = \frac{H_1 r_t}{180(d + w_t)^8} - \frac{H_2 r_t}{6(d + w_t)^2}, \tag{19}$$

where H_1 and H_2 are the Hamaker constants for the attractive and repulsive potentials, r_t is the tip-radius and $w_t = w(L_s, t)$ is the tip displacement amplitude (Rutzel et al., 2003).

Therefore, the coupled model accounts for the mass contributions of the cantilever beam, probe tip and PZT actuator, the stiffness contributions of the cantilever beam and PZT actuator, equivalent force vector due to applied electric voltage in the PZT actuator (at left-end) and force vector due to the interaction between probe tip and sample surface (at right-end).

MODEL VALIDATION AND DAMPING ESTIMATION

In real AFM operation, before starting the scanning process, a procedure called tuning is performed in order to obtain the cantilever beam frequency response and natural frequencies. Using this data, together with geometrical measures obtained via Scanning Electron Microscopy (SEM), provided by the Thin Film Laboratory of the Physics Institute of the University of São Paulo, a validation of the mathematical model, including effective damping estimation is performed.

VALIDATION OF THE MATHEMATICAL MODEL

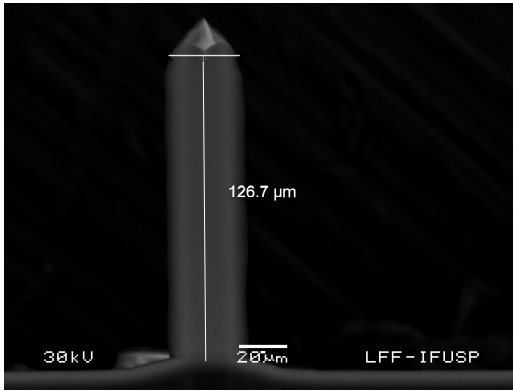The geometric parameters were taken using the images shown in Figs. 4 and 5.
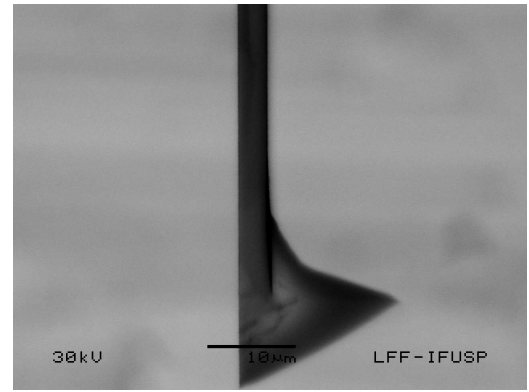
Figure 4 – Cantilever beam view.

Figure 5 – Cantilever probe tip view
.

Besides the values obtained through the SEM images, in order to fit the resonant frequencies of the system, a numerical estimation of the values of the tip base radius and tip height (R_t and h_t), as well as the PZT actuator radius and height (R_p and h_p) were performed. The interaction values of H_1 and H_2 were taken from Rutzel et al. (2003) and, along with other values, are shown in Tab. 1.

Table 1 – Known material parameters and estimated geometrical parameters based on SEM images for an AFM cantilever.

Parameter	Symbol	Value	Unit
Length of cantilever beam	L_s	127	μm
Width of the cantilever beam	b_s	33	μm
Thickness of the cantilever beam	h_s	3.37	μm
Cantilever beam Young Modulus	E_s	176×10^9	N/m^2
Cantilever beam density	ρ_s	2330	Kg/m^3
Second moment of area	I_s	105.25	μm^4
Tip base radius	R_t	11.6	μm
Tip radius	r_t	150	nm
Tip height	h_t	17.4	μm
Tip mass	m_t	5.6×10^{-12}	Kg
Tip moment of inertia	I_t	23.4×10^{-22}	Kgm^2
PZT thickness	h_p	0.0129	m
PZT radius	R_p	3×10^{-2}	m
Piezoelectric constant	e_{p33}	23.3	C/m^2
Stiffness elastic coefficient	c_{p33}^E	4.8309×10^{10}	N/m^2
Dielectric permittivity constant	$\epsilon_{p33}^\varepsilon$	1.3×10^{-8}	C/Vm
PZT mass density	ρ_p	7500	kg/m^3
Repulsive Hammaker constant	H_1	1.3956×10^{-16}	Jnm^6
Attractive Hammaker constant	H_2	865×10^{-19}	J

Figure 6 presents both experimental and numerical frequency curves and it is possible to observe that the peaks are very similar, with nearly coincident resonance frequency. First, it was desired to match the resonance frequency, regardless of the curve bell shape. The peak frequency obtained via experimental tuning of a real AFM was 225.45kHz, and the peak frequency obtained via numerical simulation is 225.14kHz, which means that the relative error between them is 0.137%, it is than concluded that the model geometric and material parameters fully meet expectations, leading to a second step that is the estimation of experimental damping factor, that will be later used in the analysis.
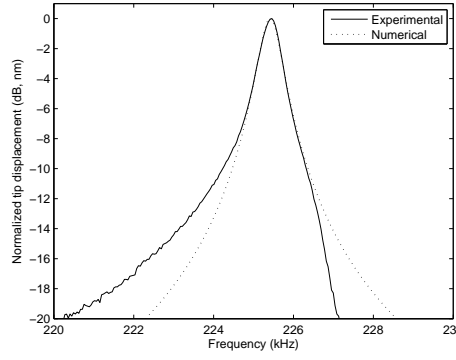
Figure 6 – Comparison between experimental data and numerical simulations

.

DAMPING ESTIMATION

The main idea of this section is to estimate the damping factor ζ of the cantilever beam using the half power bandwidth method ($-3dB$). Therefore, a procedure called sensitivity was performed in the AFM in order to obtain the cantilever beam Q-factor, which will be used to validate the result obtained via half power bandwidth method. Applying the half power bandwidth method in the obtained experimental frequency curve, follows that $\omega_0 = 225.46kHz$, $\omega_1 = 225.10kHz$ and $\omega_2 = 225.73kHz$.
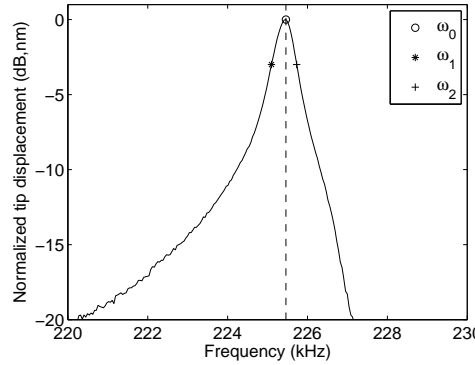
Figure 7 – Half power bandwidth method to estimate the equivalent damping factor

The estimation of damping factor ζ may be performed as follows

$$\zeta = \frac{\omega_2 - \omega_1}{2\omega_0} = 0.0014, \tag{20}$$

which means that the cantilever beam has an equivalent damping factor of 0.14%. Using the experimental acquired value of the cantilever beam Q-factor, $Q = 358$, is also possible to estimate the ζ damping coefficient,

$$\zeta = \frac{1}{2Q} = 0.0014. \tag{21}$$

With the results of Eqs. 20 and 21, it is assumed that $\zeta = 0.14\%$ will be adopted in the model for future simulations in order to analyse the dynamic behavior of the system.

## ANALYSIS OF THE NUMBER OF VIBRATION MODES TO BE RETAINED IN THE REDUCED MODEL

In this section, an analysis of the number of vibration modes that should be retained in a reduced order model, in order to properly capture the dynamic behavior of the system is performed. For that, an excitation through the PZT actuator, in the form of a sinusoidal applied electric voltage $V_p = \tilde{V}_p sin(\omega t)$ with $\tilde{V}_p = 11.492V$ and $\omega = 202.63kHz$ is considered. The frequency response function of the probe tip displacement is evaluated for different tip sample initial distances d.

The horizontal set of results in the figure 8 shows the frequency responses of the probe tip for different tip-sample distances ($d = (91, 89, 86, 64)nm$), while the vertical set represents the system response considering increasing the number of vibration modes retained in the reduced-order model. It is noticeable that, within the frequency range considered

$(100 - 600kHz)$, three peaks can be easily observed for the higher tip-sample distance, except for the model with only one vibration mode, that showed to be very limited. The second and third peaks are due to the first and second resonance frequencies of the system, whereas the first peak is due to the excitation frequency. That is why, when considering only the first vibration mode in the reduced model, the third peak is not observed. Moreover, the more the tip-sample distance is reduced the more important becomes the nonlinear interaction between vibration modes, because of the increasing effect of the tip-sample interaction forces.

This leads to both a disturbance of the frequency responses curves and also a modification of the displacement distribution along the beam span. For the latter reason, the reduced-order model with only the first vibration mode was not able to account for the local deformation of the beam tip and did not converge even for relative high tip-sample distances ($86nm$), for this reason, there is no results for $d = (86, 64nm)$, fact noticed with the presence of two blanks in the first horizontal line. The same behavior was observed for the other reduced models, such that the two modes model stopped converging for tip-sample distances smaller than $86nm$, and the three modes model stop converging for tip-sample distances smaller than $64nm$. With four vibration modes, the model converged even for very low tip-sample distances (smaller than $1nm$), and, thus, it is suggested that a reduced-order model with the first four vibration modes is satisfactory and shall be used for following analyses.
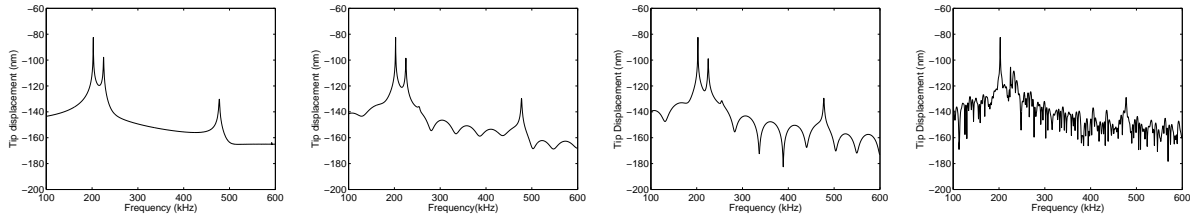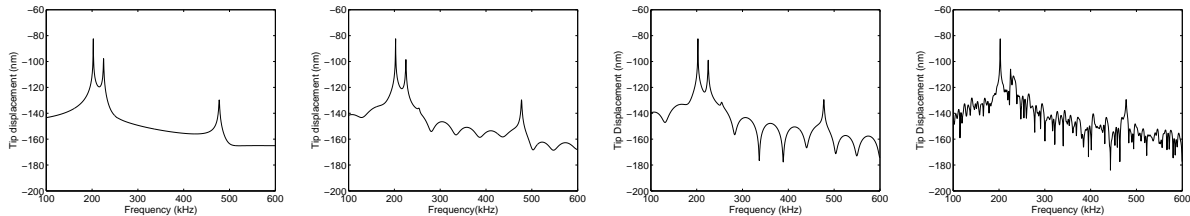
Mode 1
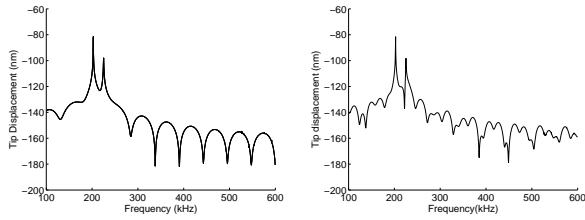
Modes $1 - 2$
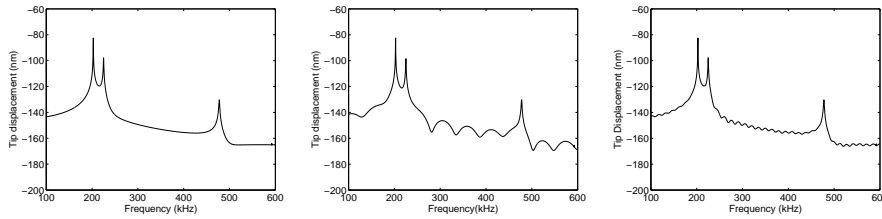

Modes $1 - 3$

Modes $1 - 4$

Figure 8 – Frequency responses of the probe tip under excitation through the PZT actuator for different tip-sample initial distances and when considering up to four vibration modes in the reduced-order model. From left to right: ($d = (91, 89, 86, 64)nm$).

## Tip-sample distance variation

The goal of this section is to observe the dynamics of the cantilever beam while the tip-sample distance d decreases. Furthermore, it will be possible to observe the influence of the intermolecular forces in the behavior and structure of the system. At the time history, with $d = 100nm$ the maximum and minimum amplitudes are $88,7nm$ and $-88,83nm$ respectively. Free from intermolecular forces, the system presents a large amplitude in the transient region. In the steady state region, the oscillation varies from $-47nm$ to $46.8nm$. With $d = 20nm$, there is the presence of interaction forces

forcing the biggest amplitude to get smaller and flattening the underside of the time history.
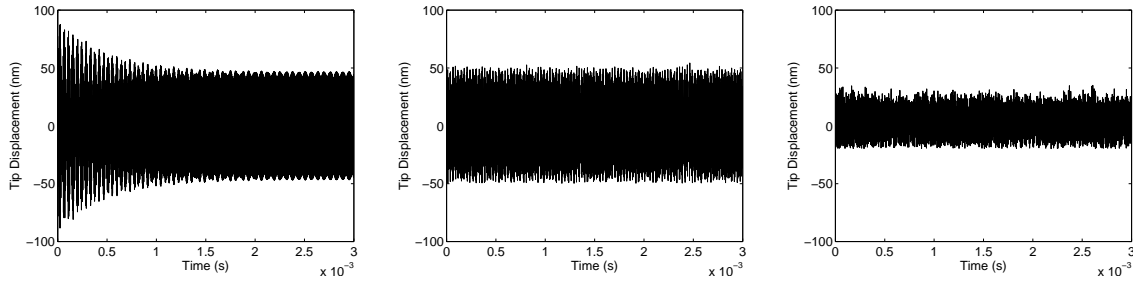
Figure 9 – Time response of the tip displacement using four-mode reduced model for different tip-sample initial distances. From left to right, $d = (100, 50, 20)nm$**.**

In the absence of the intermolecular forces ($d = 100nm$), three different peaks are clearly observed, the first being due to the excitation frequency and the other due to the first two resonant frequencies. For $d = 50nm$, the response starts to become very noise and several other peaks seem to appear.
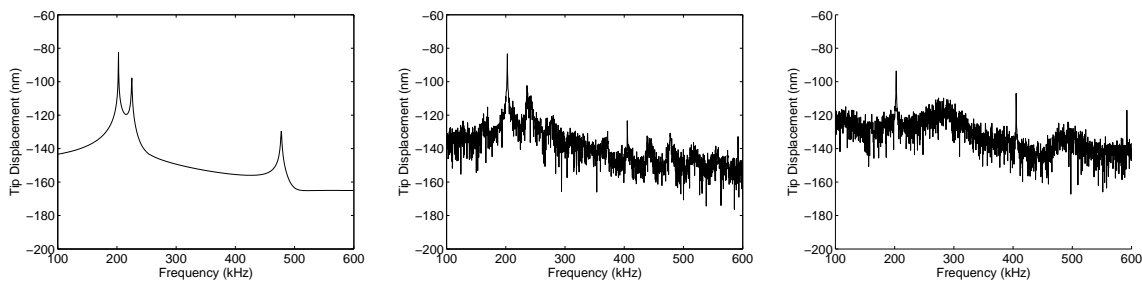
Figure 10 – Frequency response of the probe tip displacement calculated using four-mode reduced model for different tip-sample initial distances, From left to right, $d = (100, 50, 20)nm$**.**

When $d = 20nm$, the only clear response peaks are due to excitation frequency and its multiples, which highlights the effect of the interaction forces in the system behavior. In Fig. 11, the frequency responses of the system with different values of d are shown and it is clear that, as the distance decreases, several peaks appear. It means that the intermolecular interactions increase while the tip-sample distance decreases. The appearance of different peaks means that the intermolecular forces change some characteristics of the cantilever beam, like the stiffness of the system.
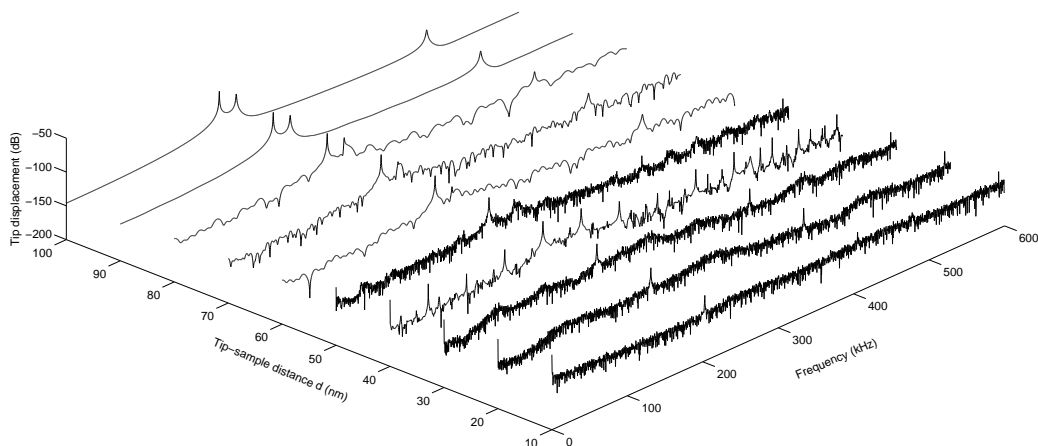
Figure 11 – Frequency response of the probe tip displacement for different tip-sample distances

The purpose of the Fig. 12 is to present a compilation of all time histories at the same simulation, point to point, as the tip-sample distance decreases. An overview of the system shows that while d decreases, the transient region disappear and the oscillation amplitude get smaller, with a flattening of the negative region, showing that the tip starts to vibrate very close to the sample surface.
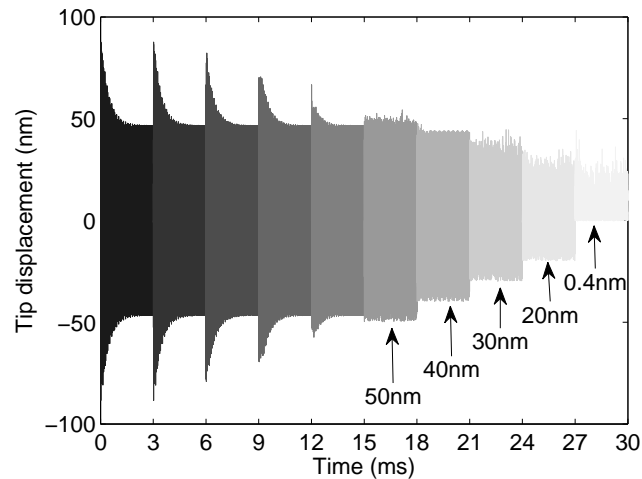
Figure 12 – Time response of the probe tip displacmeent with different tip-sample distances

It is also possible to conclude that the method used to obtain this result is very similar to the method used by the AFM to obtain the point-to point interactions.

CONCLUSIONS AND FUTURE WORKS

The main idea of this work was to present a model to represent the system composed by the PZT base, cantilever beam with tip mass under the influence of interaction forces. The obtained model presented good results when compared with experimental ones. The validation was successfully realized, with small difference between the resonant peak of experimental data and numerical simulation. The analysis performed varying the number of vibration modes showed that the system considering only one vibration mode (1 dof) does not present reasonable results. With respect to the variation of the tip distance, the system proved to be extremely sensitive to the presence of the forces of attraction and repulsion. After these analyses, it is possible to conclude that the presented model is satisfactory for modeling the AFM system, with easy computational implementation, and enabling a wide range of settings and analysis.

ACKNOWLEDGEMENTS

REFERENCES

1

Claeyssen, J.R., 2010. "The Timoshenko Model in Atomic Force Microsocopy". Proceedings of 9th Brazilian Conference of Dynamics and Their Applications (DINCON).

Dankowicz, H., 2006. "Nonlinear dynamics as an essential tool for non-destructive characterization of soft nanostructures using tapping-mode atomic force microscopy." Philosophical transactions. Series A, Mathematical, physical, and engineering sciences, Vol. 364, No. 1849, pp. 3505–20.

Hsu, J.C., Lee, H.L. and Chang, W.J., 2007. "Flexural vibration frequency of atomic force microscope cantilevers using the timoshenko beam model". Nanotechnology, Vol. 18, No. 28, p. 285503. URL http://stacks.iop.org/0957-4484/18/i=28/a=285503.

Israelachvli, J.N., 1991. Intermolecular and Surface Forces. Academic Press, 2nd edition.

Jalili, N. and Laxminarayana, K., 2004. "A review of atomic force microscopy imaging systems: application to molecular metrology and biological sciences". Mechatronics, Vol. 14, No. 8, pp. 907–945.

Misra, S., Dankowicz, H. and Paul, M.R., 2008. "Event-driven feedback tracking and control of tapping-mode atomic force microscopy". Proceedings of the Royal Society A: Mathematical, Physical and Engineering Sciences, Vol. 464, No. 2096, pp. 2113–2133.

Nozaki, R., Balthazar, J.M. and Tusset, A.M., 2010. "Optimal linear control to an atomic force microscope (afm) problem with chaotic behavior". In Proceedings of 9th Brazilian Conference of Dynamics and Their Applications (DINCON). Serra Negra, SP, pp. 371–377.

Rodrigues, K.d.S., Balthazar, J.M., Tusset, A.M., de Pontes, Bento Rodrigues, J. and Bueno, t.M., 2014. "Preventing chaotic motion in tapping-mode atomic force microscope". Journal of Control, Automation and Electrical Systems, pp. 1–9.

Rodrigues, K.S., Balthazar, J.M., Tusset, A.M. and Pontes Jr., B.R., 2011. "Dynamical study of a piecewise-smooth model in tapping mode atomic force microscope". Proceedings of 10th Brazilian Conference of Dynamics and Their Applications (DINCON).

Rutzel, S., Lee, S.I. and Raman, A., 2003. "Nonlinear dynamics of atomic-force-microscope probes driven in Lennard-Jones potentials". Proceedings of the Royal Society A: Mathematical, Physical and Engineering Sciences, Vol. 459, No. 2036, pp. 1925–1948.

Stark, R., Schitter, G., Stark, M., Guckenberger, R. and Stemmer, A., 2004. "State-space model of freely vibrating and surface-coupled cantilever dynamics in atomic force microscopy". Physical Review B, Vol. 69, No. 8, pp. 1–9.

Tusset, A.M., Bueno, A.M., Nascimento, C.B., dos Santos Kaster, M. and Balthazar, J.M., 2013. "Nonlinear state estimation and control for chaos suppression in mems resonator". Shock and Vibration, Vol. 20, No. 4, pp. 749–761.

RESPONSIBILITY NOTICE

The authors are the only responsible for the material included in this paper.